Crystal structure and electronic states of the low-dimensional $S = \frac{1}{2}$ system MgV_2O_5

1998 J. Phys.: Condens. Matter 10 1229

(http://iopscience.iop.org/0953-8984/10/6/006)

J. Phys.: Condens. Matter **10** (1998) 1229–1236. Printed in the UK PII: S0953-8984(98)88775-4

Crystal structure and electronic states of the low-dimensional $S = \frac{1}{2}$ system MgV_2O_5

Masashige Onoda and Akira Ohyama

Institute of Physics, University of Tsukuba, Tennodai, Tsukuba 305, Japan

Received 28 October 1997

Abstract. The crystal structure of MgV_2O_5 has been determined by x-ray four-circle diffraction. The crystal data at 296 K indicate an orthorhombic structure with space group $Cmcm$; $a = 3.692(1)$ Å, $b = 9.971(1)$ Å, $c = 11.018(1)$ Å, and $Z = 4$. Full-matrix least-squares refinement gives the residual factors $R = 0.038$ and $R_w = 0.027$ for 976 independent reflections with the internal consistency $R_{\rm int} = 0.029$. The V zigzag chains are formed along the a-axis by sharing edges and corners of VO_5 pyramids, and the corner-sharing linkage between the chains along the c-axis leads to quasi-two-dimensional layers which stack alternately along the b-axis. The electronic states have been explored through magnetization and EPR measurements. A Curie–Weiss-type paramagnetism with $g \simeq 1.96$ is present above 300 K, while at low temperatures, short-range-order effects appear with a critical contribution of the EPR linewidth. This is clearly different from the spin-gap properties of CaV_2O_5, which may be attributed to a significant change in the path of superexchange interaction between the chains.

1. Introduction

Spin-singlet ground states often appear in transition-metal ternary oxides or bronzes with unfilled 3d orbitals [1–7]. The singlet bipolaronic state in a quasi-one-dimensional conductor $Na_{0.33}V_2O_5$ [1] and the singlet trimerized state in a triangular-lattice conductor $LiVO_2$ [2] are formed accompanied with lattice distortions due to electron (spin)–phonon couplings. The Haldane state or the valence-bond solid in one-dimensional magnets is due to quantum spin-fluctuation effects, which may also be responsible for the spin-gap state in the ladder compounds with $S = \frac{1}{2}$ [4]. Recently, the characteristic spin gap in a two-dimensional magnet CaV_4O_9 which is a member of the CaV_nO_{2n+1} system with V^{4+} ($3d^1$) has been explored from the experimental [5] and theoretical viewpoints [8].

CaV_2O_5 which corresponds to $n = 2$ in the above system has a spin gap that appears to be characterized by a simple dimer model rather than the model of quadratic energy dispersion with the finite gap [7]. This compound is orthorhombic with space group $Pmmn$ and the lattice constants are $a = 11.351(2), b = 3.604(1)$, and $c = 4.893(1)$ Å. The V zigzag chains are formed along the b-axis by sharing edges and corners of VO_5 pyramids. They are also linked in the normal direction by sharing corners, which leads to a quasi-two-dimensional layer. As far as the room temperature structure is concerned, no lattice distortion that can be related to a dimerized state in the zigzag chain has been observed. If the V ions for interchain bonds are bound, the spin gap could be basically explained without invoking quantum effects. However, this model neglects possible contributions from superexchange interactions in the zigzag chains.

0953-8984/98/061229+08$19.50

CaV_2O_5 has been considered as a spin ladder on the basis of NMR results [6]. Here, the spin-gap energy for the Knight shift K of the ^{51}V nuclei was apparently different from that for the spin–lattice relaxation rate T_1^{-1}. However, it should be noted that our dimer model [7] accounts for both previous results for K and T_1^{-1} with the *same* energy. When the spin-ladder model is applied, the magnetic properties of CaV_2O_5 should be interpreted as those of isolated rung dimers as described above.

There are several compounds having the chemical formula MV_2O_5, where M is an alkaline or alkaline-earth element. MgV_2O_5 with V^{4+} is C-centred orthorhombic and the lattice constants are $a = 3.696(3)$, $b = 9.965(5)$, and $c = 11.019(5)$ Å [9]. No detailed crystal structure has been determined. However, from the comparison of the lattice constants of MgV_2O_5 and CaV_2O_5, these compounds are expected to have a similar layer, though a pile of layers of MgV_2O_5 may be modified due to the doubling of the interlayer distance.

In order to fully describe the anomalous spin-singlet states of CaV_2O_5, it is important to explore structural and electronic aspects for members of the system with similar structures. This work describes the precise crystal structure of MgV_2O_5 determined by means of x-ray four-circle diffraction as well as the electronic states revealed through magnetization and EPR measurements.

Table 1. Atomic coordinates, equivalent isotropic thermal parameters B_{eq} (Å^2), and anisotropic displacement parameters U_{ij} of MgV_2O_5 at 296 K, where $x = 0$ and $U_{12} = U_{13} = 0$ for all of the atoms. B_{eq} and U_{ij} are defined as $B_{eq} = \frac{8}{3}\pi^2[U_{11}(aa^*)^2 + U_{22}(bb^*)^2 + U_{33}(cc^*)^2 + 2U_{12}aa^*bb^*\cos\gamma + 2U_{13}aa^*cc^*\cos\beta + 2U_{23}bb^*cc^*\cos\alpha]$ and $T = \exp[-2\pi^2(a^{*2}U_{11}h^2 + b^{*2}U_{22}k^2 + c^{*2}U_{33}l^2 + 2a^*b^*U_{12}hk + 2a^*c^*U_{13}hl + 2b^*c^*U_{23}kl)]$, respectively.

Atom	y	z	B_{eq}	U_{11}	U_{22}	U_{33}	U_{23}
V	0.201 94(4)	0.097 00(4)	0.458(4)	0.0065(1)	0.0064(1)	0.004 48(9)	0.0001(1)
Mg	0.1132(1)	$\frac{3}{4}$	0.64(2)	0.0079(5)	0.0071(5)	0.0092(5)	—
O1	0.0432(2)	0.1275(2)	1.19(3)	0.027(1)	0.0080(7)	0.0103(7)	0.0016(6)
O2	0.2358(2)	−0.0792(1)	0.63(2)	0.0066(6)	0.0118(7)	0.0055(6)	−0.0003(5)
O3	0.3044(3)	$\frac{1}{4}$	0.54(3)	0.0078(8)	0.0064(8)	0.0062(7)	—

2. Crystal structure

2.1. Experiments and crystal data

Polycrystalline specimens of MgV_2O_5 were prepared as follows: mixtures of 2MgO (99.99% purity), V_2O_5 (99.99% purity), and V_2O_3 that was made according to the procedure described in reference [10] were ground and pressed into pellets. They were sealed in quartz tubes and then heated at 1173 K for five days. The pellets obtained were covered thinly with dark blue powders. On removing these powders, green specimens were obtained. X-ray powder diffraction patterns for the green specimens measured at 296 K on a two-circle diffractometer with Cu Kα radiation indicated a single phase, while the blue powders contained VO_2. The single crystals used in the structure analysis were obtained by annealing the polycrystalline specimens under an Ar atmosphere at 1223 K with several intermediate grindings. Above 1223 K, the specimens further decomposed into several phases. MgV_2O_5 is an insulator.

The x-ray four-circle diffraction measurements were performed at 296 K on a Rigaku AFC-7R diffractometer (custom-made) with graphite-monochromated Mo Kα radiation and

a 18 kW rotating-anode generator. A crystal with dimensions $0.04 \times 0.02 \times 0.04$ mm was mounted on a glass fibre. The intensity data for the structure analysis were collected over the wide range of $2\theta = 120^\circ$ using the ω–2θ scan technique. Of 1761 unique reflections, 976 reflections with $|F_o| \geqslant 3\sigma$ were used. Lorentz polarization was applied. Due to the small size of the crystal, no absorption correction was applied; this was proved to be justified by azimuthal scans of several reflections. The internal consistency of the reflections was estimated to be $R_{int} = 0.029$ under the condition $2\theta \leqslant 60^\circ$.

Through the systematic absences of reflections, a statistical analysis of the intensity distribution, and the successful solution and refinement of the structure, the following crystal data were determined: orthorhombic with space group $Cmcm$ (No 63); $a = 3.692(1), b = 9.971(1), c = 11.018(1)$ Å, $V = 405.60(9)$ Å^3, $Z = 4$; μ(Mo Kα) $= 4.660$ mm^{-1}, and $D_{cal} = 3.376$ Mg m^{-3}.

2.2. Structure determination and discussion

The structure was determined by direct methods [11], expanded using Fourier techniques, and refined by means of full-matrix least-squares calculations with anisotropic displacement parameters. Here, atomic scattering factors and anomalous dispersion effects were included [12, 13]. The final residual factors defined as

$$R = \sum(|F_o| - |F_c|)^2 \Big/ \sum |F_o|$$

and

$$R_w = \left[\sum w(|F_o| - |F_c|)^2 \Big/ \sum w F_o^2\right]^{1/2}$$

are $R = 0.038$ and $R_w = 0.027$. All of the calculations were performed using the teXsan crystallographic software package [14].

Table 2. Selected interatomic distances (Å) of MgV_2O_5, where the translation codes are (i) x, y, z; (ii) $-\frac{1}{2} + x, \frac{1}{2} - y, -z$; (iii) $\frac{1}{2} + x, \frac{1}{2} - y, -z$; (iv) $x, y, \frac{1}{2} - z$; (v) $-\frac{1}{2} + x, \frac{1}{2} - y, -\frac{1}{2} + z$; (vi) $x, -y, \frac{1}{2} + z$; (vii) $x, -y, 1 - z$; (viii) $x, y, 1 + z$; (ix) $-\frac{1}{2} + x, \frac{1}{2} - y, \frac{1}{2} + z$; (x) $\frac{1}{2} + x, \frac{1}{2} - y, \frac{1}{2} + z$.

VO_5 pyramid		Edges of pyramid		Others	
V(i)–O1(i)	1.618(2)	O1(i)–O2(i)	2.979(3)	V(i)–V(ii)	2.9825(7)
V(i)–O2(i)	1.971(2)	O1(i)–O3(i)	2.933(3)	V(i)–V(iv)	3.3716(8)
V(i)–O2(ii, iii)	1.9575(8)	O1(i)–O2(ii, iii)	2.923(2)	V(i)–Mg(v)	3.106(1)
V(i)–O3(i)	1.971(2)	O2(i)–O2(ii, iii)	2.556(2)	Mg(i)–O1(vi, vii)	2.063(2)
—		O3(i)–O2(ii, iii)	2.666(1)	Mg(i)–O2(iv, viii)	2.244(2)
—		—		Mg(i)–O3(ix, x)	2.021(1)

The atomic coordinates, equivalent isotropic thermal parameters, and anisotropic displacement parameters are listed in table 1. Selected interatomic distances are listed in table 2. The crystal structures projected on the ac- and bc-planes are shown in figures 1(a) and 1(b), respectively. The structure can be described as a linkage of VO_5 pyramids having apex oxygens in the direction of the b-axis. The displacement parameters for entire atoms may be in the normal range. The V zigzag chains extend along the a-axis by sharing edges and corners of the pyramids, where the nearest-neighbour V–V distance is 2.98 Å. They

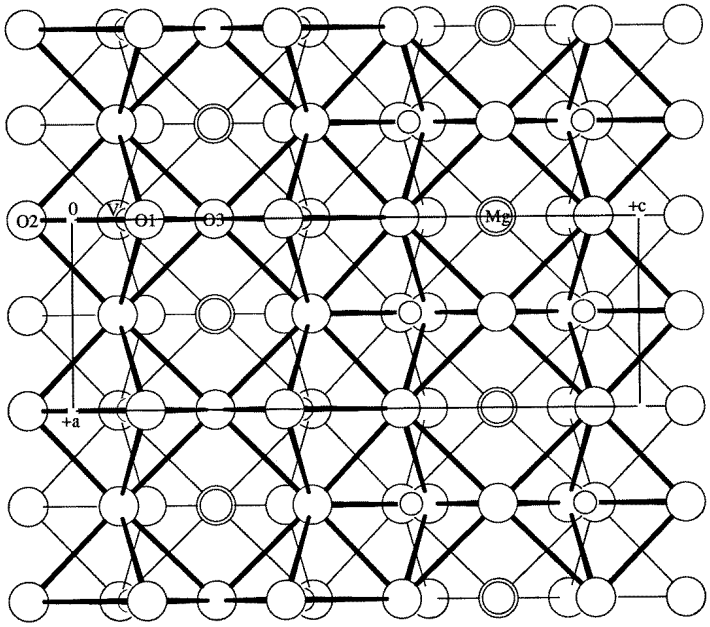

(*a*)

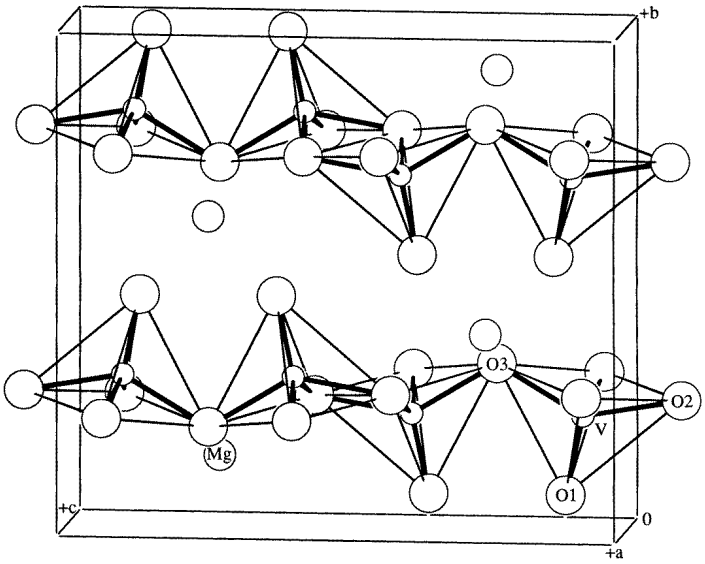

(*b*)

Figure 1. The crystal structure of MgV_2O_5 at 296 K projected onto (*a*) the *ac*-plane and (*b*) the *bc*-plane. The thick and the thin lines for the basal plane of the oxygen pyramids in (*a*) correspond to the edges at $y \sim 0.27$ and $y \sim 0.77$, respectively.

are also linked by sharing corners, with the V–V distance of 3.37 Å, which leads to quasi-two-dimensional layers in the *ac*-plane. These layers stack alternately with the distance of $b/2$. Mg atoms are located between the layers and each surrounded by six O atoms.

By using the bond length versus bond strength relation [15], the effective valence at the V site is estimated to be 4.0, which is consistent with V^{4+} ($3d^1$) expected from the chemical formula. The ground-state wavefunction of d^1 for the VO_5 pyramid is mainly composed of $0.853d_{xy} + 0.504d_{yz}$, where $x \parallel c$ and $y \parallel a$, in terms of simple crystal-field analysis with the Hartree–Fock function for V^{4+} [16]. From table 2, the V–O–V angles responsible for the superexchange interactions are estimated as follows. For the edge- and corner-sharing path in the zigzag chain, the respective angles are 98.80(5)° and 141.1(1)°. The angle for the corner-sharing path between the chains is 117.6(1)°. The average Mg–O distance for MgO_6 is 2.11 Å, which is consistent with the value for six-coordinated Mg ions [17].

Although the two-dimensional layer of MgV_2O_5 is roughly similar to that of CaV_2O_5 [7], several significant differences as regards the V–V distance and the V–O–V angle exist there: for CaV_2O_5, the V–V distance in the chain is 3.03 Å and that between the chains is 3.49 Å; and the V–O–V angles for the edge and corner linkages in the chain are 100.7° and 135.3°, respectively, and that between the chains is 132.9°. This should lead to different superexchange interactions and hence also different magnetic properties. A comment on the correlation between the crystal structure and the magnetic properties will be made in section 4.

3. Electronic states

3.1. Experiments

The magnetizations with a field of up to 1 T for the polycrystalline specimens were measured by the Faraday method between 4.2 and 900 K. The magnetization–field curve was linear, and thus the magnetic susceptibility was deduced from that slope. EPR measurements were also performed at 9.199 GHz using a JEOL spectrometer between 14 and 300 K.

3.2. Results and discussion

The magnetic susceptibility χ against temperature is shown in figure 2(a). It has a Curie–Weiss-type temperature dependence above 300 K: $\chi = C/(T + T_W) + \chi_0$, where C, T_W, and χ_0 are, respectively, the Curie constant, Weiss temperature, and the temperature-independent contributions from the Van Vleck orbital and diamagnetic susceptibilities. The full curve in figure 2(a) is based on the parameters $C = 0.359$ emu K (mol V)$^{-1}$, $T_W = 174$ K, and $\chi_0 = 2 \times 10^{-5}$ emu (mol V)$^{-1}$. This Curie constant corresponds to $g = 1.959$ assuming that $S = \frac{1}{2}$, which is justified for the EPR results as will be shown later. When the superexchange interaction through an edge-sharing path is written as J_e and those through corner-sharing paths along the a- and c-axes are J_{c1} and J_{c2}, respectively [18], T_W is expressed as $J_e/2 + J_{c1}/2 + J_{c2}/4$.

Below 300 K, the temperature dependence of the susceptibility deviates from the full curve and has a broad peak at 107 K, as expected for low-dimensional spin systems. For example, a linear-chain model formulated by Bonner and Fisher [19] roughly explains the temperature dependence of the susceptibility above 40 K. However, the Curie constant obtained, $C = 0.271$ emu K (mol V)$^{-1}$, is much smaller than that estimated from the Curie–Weiss law above 300 K due to the model being oversimplified. At lower temperatures, the susceptibility decreases considerably, and is roughly proportional to T^2 at temperatures below 15 K as shown in figure 2(b), which indicates that MgV_2O_5 does not have a spin-singlet ground state. The extrapolated susceptibility at 0 K is half of the molecular-field value for antiferromagnetic states without quantum spin-fluctuation effects based on the

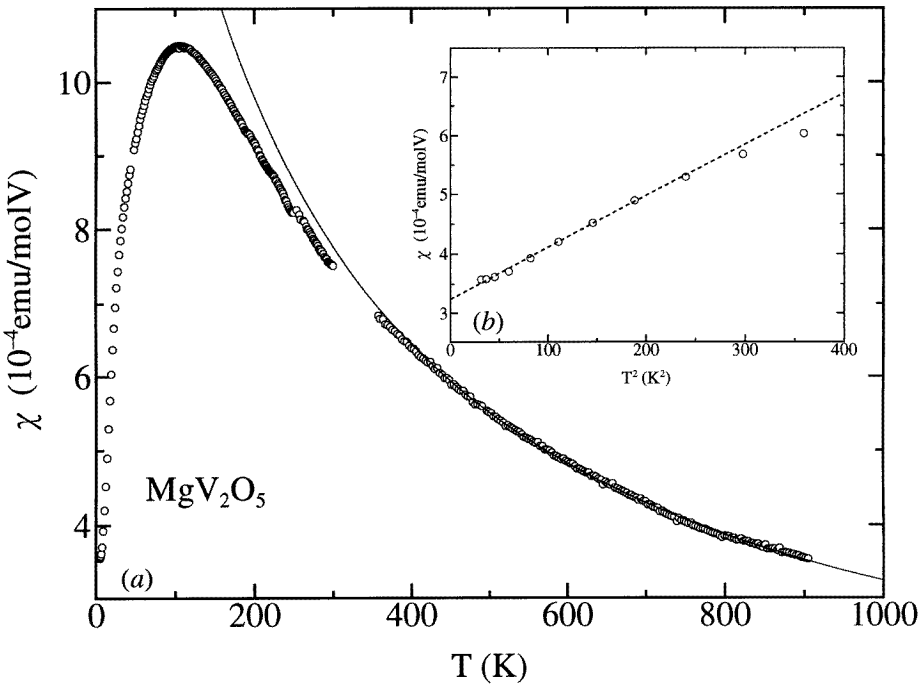

Figure 2. The temperature dependence of the magnetic susceptibility χ of MgV_2O_5: (*a*) χ against T and (*b*) χ against T^2, where the full curve indicates the calculated result based on a Curie–Weiss law.

above T_W- and g-values.

The EPR signal at high temperatures is apparently a single Lorentzian as shown in figure 3(*a*). The extracted spin susceptibility is comparable with the static susceptibility, which is consistent with the above result that the major component of the static susceptibility comes from spins. At low temperatures, another signal with small linewidth appears, which probably originates from lattice imperfections or impurities that cannot be detected by means of standard x-ray powder diffraction, because the intensity relative to that of the intrinsic Lorentzian signal with larger linewidth is of the order of 10^{-3} above 50 K. The temperature dependence of the peak-to-peak linewidth W of the absorption derivatives of the intrinsic signals is shown in figure 3(*b*). With a decrease of temperature, the linewidth increases and has a maximum at 40 K and then decreases. In the temperature region where the linewidth is comparable with the resonance field, the signal shape shows significant departures from the classical Lorentzian shape. This is not due to the so-called low-field effect [20], but due to the mixture of dispersive components for non-negligible magnetic losses [21]. The thick curves in figure 3(*a*) are the results calculated under these conditions. The g-factor is nearly temperature independent, $g \simeq 1.96$, in the region for which measurements were made, which is similar to the values for CaV_2O_5 [7], NaV_2O_5 [22], and MV_3O_7 (M = Cd, Ca, and Sr) [23]. These compounds have similar VO_5 pyramids and all have the d_{xy}-type ground-state wavefunction.

The linewidth is generally a measure of the relaxation rate for spin fluctuations perpendicular to the static field, although its analysis is complicated by the effect of the field on the spin dynamics. An increase in the linewidth and the extraordinarily large linewidth

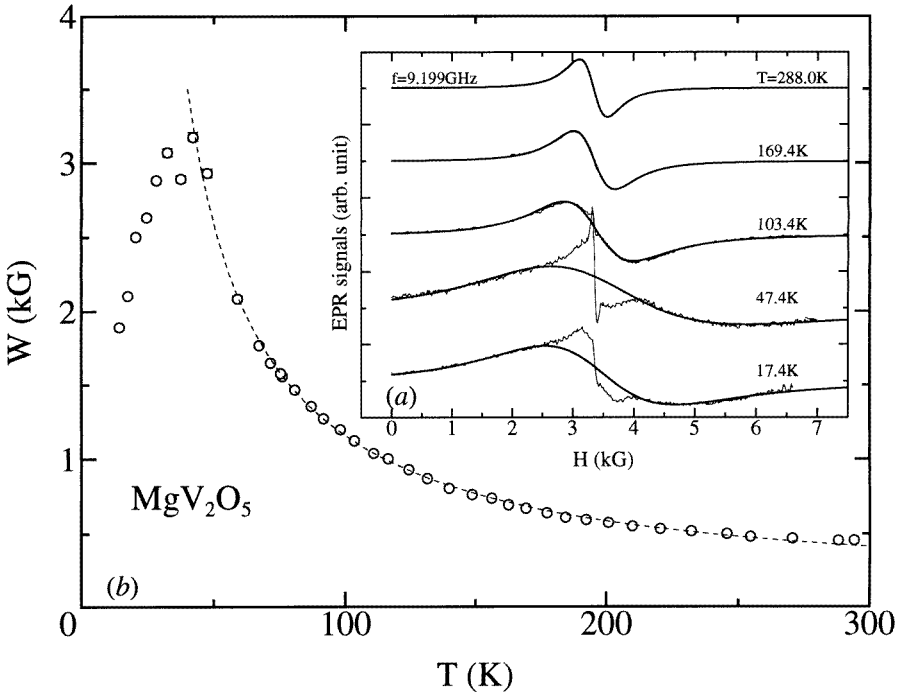

Figure 3. (*a*) EPR signals of MgV_2O_5 at several temperatures, where the thin and thick curves represent the experimental and calculated results, respectively, and (*b*) the temperature dependence of the linewidth W, where the broken curve indicates the critical contribution.

at low temperatures seem to correspond to the critical slowing down of the spins. This contribution is empirically expressed as $W - W_\infty \propto (T - T^*)^{-1}$, where W_∞ is the limiting value at high temperatures, and T^* is the critical temperature [24]. The data above 40 K are described well by this relation as indicated by the dotted curve, where $W_\infty \simeq 8$ mT and $T^* \simeq 13$ K. Using a correlation time roughly expressed as $\tau_c \simeq h/T_W$ [25], h being Planck's constant, the powder-averaged linewidth due to the moments arising through the interplay of the exchange interaction and the dipole–dipole coupling between spins [26] is estimated to be 0.2 mT, which is an order of magnitude smaller than W_∞. Here, the contribution from the hyperfine coupling [27] is negligible. The *paramagnetic* behaviour between T^* and 40 K is different from the usual critical contribution, and thus could be interpreted as indicating a short-range-order spin cluster or the effects of frustration on the characteristic V lattice.

4. Conclusion

The crystal structure and electronic states of MgV_2O_5 have been explored through measurements of x-ray four-circle diffraction, magnetization, and EPR.

This compound has a similar two-dimensional layer, formed by the linkage of VO_5 pyramids, to that of CaV_2O_5. However, both the V–V distances and the V–O–V angles are significantly modified. The arrangement of layers in the normal direction also changes. The magnetic properties above 300 K are explained by a Curie–Weiss law with $g \simeq 1.96$, while at

low temperatures, short-range magnetic order effects appear with a critical contribution of the EPR linewidth. Here, it is necessary to clarify whether MgV_2O_5 remains paramagnetic due to the frustration effects or has magnetic order due to the three-dimensional spin correlation. On the other hand, CaV_2O_5 exhibits spin-gap properties. Thus, the structural modification in the layer causes a clear difference between the electronic states of CaV_2O_5 and MgV_2O_5. Here, the largest change in the V–V distances and the V–O–V angles responsible for the path of the superexchange interactions in these compounds may be in the corner-sharing linkage between the zigzag chains. This will lead to a reduction of the transfer integral between the chains in MgV_2O_5, which may enhance the low-dimensional spin properties.

References

[1] Onoda M and Nagasawa H 1987 *Phys. Status Solidi* b **141** 507
[2] Onoda M and Inabe T 1993 *J. Phys. Soc. Japan* **62** 2216
[3] Mur J and Darriet J 1985 *C. R. Acad. Sci., Paris* **300** 599
[4] Dagotto E and Rice T M 1996 *Science* **271** 618 and references therein
[5] Kodama K, Harashina H, Sasaki H, Kobayashi Y, Kasai M, Taniguchi S, Yasui Y, Sato M, Kakurai K, Mori T and Nishi M 1997 *J. Phys. Soc. Japan* **66** 793 and references therein
[6] Iwase H, Isobe M, Ueda Y and Yasuoka H 1996 *J. Phys. Soc. Japan* **65** 2397
[7] Onoda M and Nishiguchi N 1996 *J. Solid State Chem.* **127** 359
[8] Fukumoto Y 1997 *J. Phys. Soc. Japan* **66** 2178 and references therein
[9] Bouloux J-C, Milosevic I and Galy J 1976 *J. Solid State Chem.* **16** 393
[10] Onoda M, Ohta H and Nagasawa H 1991 *Solid State Commun.* **79** 281
[11] Hai-Fu F 1991 *SAPI91: Structure Analysis Programs with Intelligent Control* (Tokyo: Rigaku Corporation)
[12] Cromer D T and Waber J T 1974 *International Tables for X-Ray Crystallography* vol 4, ed J A Ibers and W C Hamilton (Birmingham: Kynoch) §2
[13] Creagh D C and McAuley W J 1992 *International Tables for Crystallography* vol C, ed A J C Wilson (Boston, MA: Kluwer Academic)
[14] teXsan 1992 *Crystal Structure Analysis Package* (The Woodlands, TX: Molecular Structure Corporation)
[15] Zachariasen W H 1978 *J. Less-Common Met.* **62** 1
[16] Freeman A J and Watson R E 1965 *Magnetism* vol 2, part A, ed G T Rado and H Suhl (New York: Academic)
[17] Shannon R D 1976 *Acta Crystallogr.* A **32** 751
[18] The Heisenberg Hamiltonian is defined as $H = J\boldsymbol{S}_i \cdot \boldsymbol{S}_j$, $\boldsymbol{S}_i$ being the spin operator at site i.
[19] Bonner J C and Fisher M E 1964 *Phys. Rev.* **135** A640
[20] Garstens M A, Singer L S and Ryan A H 1954 *Phys. Rev.* **96** 53
[21] Seehra M S 1968 *Rev. Sci. Instrum.* **39** 1044
[22] Ogawa K, Onoda M and Nagasawa H 1986 *J. Phys. Soc. Japan* **55** 2129
[23] Onoda M and Nishiguchi N 1997 unpublished results
[24] Huber D L 1972 *Phys. Rev.* B **6** 3180
[25] Moriya T 1956 *Prog. Theor. Phys.* **16** 641
[26] Abragam A 1961 *The Principles of Nuclear Magnetism* (Oxford: Oxford University Press)
[27] Ioffe V A and Patrina I B 1968 *Sov. Phys.–Solid State* **10** 639